Author Accepted Manuscript version of the paper by Wang, Weizhi; Pakozdi, Csaba; Kamath, Arun; Bihs, Hans. Representation of 3-h Offshore Short-Crested Wave Field in the Fully Nonlinear Potential Flow Model REEF3D::FNPF. Journal of Offshore Mechanics and Arctic Engineering 2022 ;Volum 144.(4)
DOI: http://dx.doi.org/10.1115/1.4053774

Representation of three-hour offshore short-crested wave field in the fully nonlinear potential flow model REEF3D::FNPF

Weizhi Wang *[1], Csaba Pákozdi[2], Arun Kamath[1], and Hans Bihs[1]

[1]Department of Civil and Environmental Engineering, Norwegian University of Science and Technology (NTNU), 7491 Trondheim, Norway
[2]SINTEF Ocean, Otto Nielsens veg 10, 7052 Trondheim, Norway

Journal of Offshore Mechanics and Arctic Engineering, 2021, -, pp. -.
DOI: http://dx.doi.org/-

---

abstract

Stochastic wave properties are crucial for the design of offshore structures. Short-crested seas are commonly seen at the sites of offshore structures, especially during storm events. A long time duration is required in order to obtain the statistical properties, which is challenging for numerical simulations. In this scenario, a potential flow solver is ideal due to its computational efficiency. A procedure of reproducing accurate short-crested sea states using the open-source fully nonlinear potential flow model REEF3D::FNPF is presented in the paper. The procedure examines the sensitivity of the resolutions in space and time as well as the arrangements of wave gauge arrays. A narrow band power spectrum and a mildly spreading directional spreading function are simulated, and an equal energy method is used to generate input waves and avoid phase-locking. REEF3D::FNPF solves the Laplace equation together with the boundary conditions using a finite difference method. A sigma grid is used in the vertical direction and the vertical grid clustering follows the principle of constant truncation error. High-order discretisation methods are implemented in space and time. Message passing interface is used for high performance computation using multiple processors. Three-hour simulations are performed in full-scale at a hypothetic offshore site with constant water depth. The significant wave height, peak period, kurtosis, skewness and ergodicity are examined in the numerically generated wave field. The stochastic wave properties in the numerical wave tank (NWT) using REEF3D::FNPF match the input wave conditions with high fidelity.

1 Introduction

Ocean waves are random by nature, and short-crested irregular waves are common near storm events. The design of marine structures and the choice of sites both depend on a good

*Corresponding author, weizhi.wang@ntnu.no

understanding of the random irregular wave condition. In many cases, the area of interest is large in space and the marine environment changes dramatically over time as well as from location to location. Experiments are expensive and lack of flexibility in such situations. Numerical models have been developed to simulate the large-scale wave propagations with flexible scenarios. Typically, a three-hour duration is needed to obtain short term wave statistical properties. In order to numerically simulate a multi-directional irregular wave field at an offshore deepwater area for three hours, an appropriate model is needed and the simulation needs to be correctly configured.

Spectral wave models such as SWAN Booij et al. (1999) are fast and efficient models that solve the energy action equations and provide the spatial distribution of wave statistical properties. However, in many cases, time domain information is needed, especially for structure responses and fatigue analysis. Here, phase-resolved models offer time series of wave kinematics and dynamics as well as the statistical properties. When the engineering application involves a large array of structures, such as fish farms and wind farms, a phase-revolved solution is needed for a large-scale domain, which requires a computationally efficient solution. Many two-dimensional wave models solving shallow water equations, such as Boussinesq-type wave models Madsen et al. (1991); Nwogu (1993) provide such solutions for shallow water regions. However, offshore platforms, fish farms and wind farms are increasingly moving to deep water, where assumptions of such models fail. Computational fluid dynamics (CFD) solves the Navier-Stokes equations for the kinematics and dynamics of fluid and is able to reproduce high fidelity wave field. However, the method requires fine resolutions in space and time and tends to become too time consuming for wave propagation simulations, especially at large-scale and with long duration.

The alternatives to achieve fast deepwater wave simulations are potential flow based numerical models. One of the widely used models is the boundary element method (BEM) model Li and Fleming (1997). Many efforts have been made to introduce nonlinearity in the model to be able to represent steep waves Grilli et al. (1994); Grilli and Horrillo (1997); Grilli et al. (2001). However, these methods tend to require the evaluation of dense matrix–vector products Brink et al. (2017), making it difficult to implement high-order numerical schemes and parallel computation techniques for large-scale long-duration wave modelling. Finite element method (FEM) based Laplace solvers have also been developed Ma et al. (2001*a*,*b*); Ma and Yan (2006). The resulting sparse system of equations is much easier to solve. However, additional numerical stabilisation or specially constructed meshes are often needed to prevent numerical instabilities Brink et al. (2017). Another field solver is based on the harmonic polynomial cell (HPC) method Shao and Faltinsen (2012, 2014*b*,*a*), where a similar sparse matrix as in the FEM models is achieved. The method has been validated for regular waves and is found to be especially useful for the studies on wave-structure interaction. For the application of large-scale irregular wave simulations, the high-order-spectrum (HOS) models Ducrozet et al. (2012); Ducrozet et al. (2016); Yates and Benoit (2015) are seen to be efficient alternatives thanks to the usage of fast Fourier transform (FFT), especially for constant water depth in the offshore waters. Short-crested seas can be generated both in a numerical wave tank (NWT) or in an open ocean condition with periodic boundary conditions. However, the representations of steep and breaking waves as well as wave transformation over complex bathymetry and coastlines are challenging and require special treatments. In comparison, finite difference method (FDM) based fully-nonlinear-potential-flow (FNPF) models Bingham and Zhang (2007); Engsig-Karup et al. (2009) are seen to be flexible alternatives.

The FDM based FNPF model REEF3D::FNPF Bihs et al. (2020) is recently introduced as a general purpose wave model that is flexible with varying bathymetry and coastlines as well as steep and breaking waves. REEF3D::FNPF is a sub-model of the open-source hydrodynamic model REEF3D Bihs et al. (2016*b*). REEF3D uses high-order discretisation schemes for the free surface and fully supports parallel computation via domain decomposition. The numerical robustness has been seen from a wide range of applications with its CFD module REEF3D::CFD, such as irregular breaking waves Aggarwal et al. (2019*a*), breaking wave interaction with a monopile Chella et al. (2019) and a jacket structure Aggarwal et al. (2019*b*). REEF3D::FNPF inherits all the high-order numerical schemes and high performance computation capacity. The model has also been used to investigate steep focused waves Wang et al. (2019).

Choosing the correct numerical wave models for a certain engineering application is important, a correct usage of numerical model is also critical. The user inputs and configurations influence the results of the simulations significantly. In the case of simulating short crested waves, the results are especially sensitive to user configurations, as many parameters play important roles in the distribution and transition of wave energy. There are several criteria to evaluate whether a simulation represents a short-crested sea state sufficiently, for example, the significant wave height, peak period, shape of the spectrum, ergodicity of the simulated wave field and the directional spreading.

The directional spreading information is usually obtained from the time series from an array of wave gauges. Similar techniques can be used both for field measurements and numerical simulations. One of the common configurations is a wave array consisting of 4 wave gauges, one in the middle, and three forming a triangle around the centric point Nwogu (1989). The method requires the least number of wave gauges. A more advanced configuration is proposed and mathematically derived Ochi (1998) with five wave gauges forming a pentagon. Several other wave gauge arrangements that consist of 4, 5 and 6 wave gauges have also been investigated Panicker and Borgman. Those arrangements have an impact on the quality of the direction spreading information obtained from a wave field though the same radius is used in each wave array. Most recently, an 8-gauge array arrangement is widely used Stansberg (1998); Tannuri et al. (2007). There, one wave gauge is located at the centre, while the other 7 wave gauges form a heptagon around the centre. A fixed radius of 0.5 m is used in this arrangement and no further correlation to wave length is explored. While the arrangement of the wave gauges in field measurements is mostly based on experience, the optimal arrangement can be straightforwardly tested thanks to the flexibility of the numerical models. However, few attempts have been made to test the configurations of wave gauges. In the numerical simulations performed by Ducrozet et. al. Ducrozet et al. (2012), 3D freak wave occurrence in a short-crested sea is examined with a truncated pentagon wave gauge arrangement Benoit and Teisson (1994). However, the radius of the wave gauge array is fixed at 1 m rather than correlated to the characteristic wavelength. In another simulation Ducrozet et al. (2016), wave number spectra are reconstructed from the free surface elevation in the entire wave tank at different time steps. Therefore, wave gauge arrangement is not studied since the analysis is not based on time series.

Due to the different numerical techniques and practices, there is a lack of a guideline to configure and evaluate a short-crested sea in a numerical wave tank. In the presented paper, the authors attempt to demonstrate a procedure of configuration and analysis to control the quality of a short-crested sea-state in a FDM based FNPF NWT using REEF3D::FNPF. Nu-

merical details regarding grid arrangements as well as the optimal radius for wave gauge arrays in correlation to characteristic wavelength are provided. Several considerations regarding the choice of the vertical grid structure and horizontal resolution for irregular waves are discussed to ensure a good representation of wave spectrum in the numerical wave model. The ergodicity of the wave field is analysed with several statistical wave properties. Finally, the directional spectrum obtained using different wave gauge arrangements are compared to investigate how the different wave gauge arrangements influence the quality of the directional spectrum in the numerical wave tank. The procedure provides insights to several key considerations in order to reproduce a multi-directional wave field with the correct energy distribution, ergodicity as well as the correct directional spreading.

2 Numerical Model

The governing equation in the open-source fully non-linear potential flow code REEF3D::FNPF is the Laplace equation:

$$\frac{\partial^2 \Phi}{\partial x^2} + \frac{\partial^2 \Phi}{\partial y^2} + \frac{\partial^2 \Phi}{\partial z^2} = 0 \tag{1}$$

Boundary conditions are needed to solve for the velocity potential Φ from this elliptic equation. At the free surface, the fluid particles remain at the surface and the pressure in the fluid is equal to the atmospheric pressure for inviscid fluid. These conditions must always hold true and they define the kinematic and dynamic boundary conditions at the free surface respectively:

$$\frac{\partial \eta}{\partial t} = -\frac{\partial \eta}{\partial x}\frac{\partial \widetilde{\Phi}}{\partial x} + \frac{\partial \eta}{\partial y}\frac{\partial \widetilde{\Phi}}{\partial y} + \widetilde{w}\left(1 + \frac{\partial^2 \eta}{\partial x^2} + \frac{\partial^2 \eta}{\partial y^2}\right), \tag{2}$$

$$\frac{\partial \widetilde{\Phi}}{\partial t} = -\frac{1}{2}\left(\frac{\partial^2 \widetilde{\Phi}}{\partial x^2} + \frac{\partial^2 \widetilde{\Phi}}{\partial y^2} - \widetilde{w}^2\left(1 + \frac{\partial^2 \eta}{\partial x^2} + \frac{\partial^2 \eta}{\partial y^2}\right)\right) - g\eta \tag{3}$$

where $\widetilde{\Phi} = \Phi(\mathbf{x}, \eta, t)$ is the velocity potential at the free surface, $\mathbf{x} = (x, y)$ represents the horizontal location and $\widetilde{w}$ is the vertical velocity at the free surface.

At the bottom, the vertical water velocity must be zero at all times since the fluid particle cannot penetrate the solid boundary. This gives the bottom boundary condition:

$$\frac{\partial \Phi}{\partial z} + \frac{\partial h}{\partial x}\frac{\partial \Phi}{\partial x} + \frac{\partial h}{\partial y}\frac{\partial \Phi}{\partial y} = 0, \quad z = -h. \tag{4}$$

where $h = h(\mathbf{x})$ is the water depth from the seabed to the still water level.

The Laplace equation and the boundary conditions are solved with a finite difference method on a σ-coordinate system. The σ-coordinate can be transferred from a Cartesian grid following:

$$\sigma = \frac{z + h\left(\mathbf{x}\right)}{\eta(\mathbf{x}, t) + h(\mathbf{x})} \tag{5}$$

In the vertical direction, the grid can be clustered towards the free surface:

$$\sigma_i = \frac{\sinh\left(-\alpha\right) - \sinh\left(\alpha\left(\frac{i}{N_z} - 1\right)\right)}{\sinh\left(-\alpha\right)}, \tag{6}$$

where α is the stretching factor and i and N_z stand for the index of the grid point and the total number of cells in the vertical direction.

Let ϕ represent the velocity potential after the σ-transformation. After ϕ is obtained, the velocities can be calculated:

$$u\left(\mathbf{x}, z\right) = \frac{\partial \phi\left(\mathbf{x}, z\right)}{\partial x} = \frac{\partial \phi\left(\mathbf{x}, \sigma\right)}{\partial x} + \frac{\partial \sigma}{\partial x}\frac{\partial \phi\left(\mathbf{x}, \sigma\right)}{\partial \sigma}, \tag{7}$$

$$v\left(\mathbf{x}, z\right) = \frac{\partial \phi\left(\mathbf{x}, z\right)}{\partial y} = \frac{\partial \phi\left(\mathbf{x}, \sigma\right)}{\partial y} + \frac{\partial \sigma}{\partial y}\frac{\partial \phi\left(\mathbf{x}, \sigma\right)}{\partial \sigma}, \tag{8}$$

$$w\left(\mathbf{x}, z\right) = \frac{\partial \sigma}{\partial z}\frac{\partial \phi\left(\mathbf{x}, \sigma\right)}{\partial \sigma}. \tag{9}$$

The Laplace equation is solved using the parallelised geometric multi-grid algorithm provided by hypre van der Vorst (1992). Second-order central differences are used for the discretisation of the Laplace equation. For the free surface, the fifth-order WENO (weighted essentially non-oscillatory) scheme Jiang and Shu (1996) is used to achieve high accuracy as well as numerical stability. For the time treatment, a third-order accurate TVD Runge-Kutta scheme Shu and Osher (1988) is used. Both fixed time step and adaptive time stepping can be applied.

The model is fully parallelised using domain decomposition strategy. Ghost cells are used to update with the values from the neighbouring processors with Message Passing Interface (MPI).

3 Irregular wave generation

The waves are generated using the relaxation method Mayer et al. (1998) with the relaxation function proposed by Jacobsen Jacobsen et al. (2012), as shown in Eqn. (10). In the wave generation zone, the free-surface elevation and velocities are increased to the designated theoretical values. In the numerical beach, a reverse process takes place and the flow properties are restored to hydrostatic values following the relaxation method. With the numerical beach, unintended wave reflection from the outlet boundary is eliminated to ensure the quality of the simulated wave field.

$$\Gamma(\widetilde{x}) = 1 - \frac{e^{(\widetilde{x}^{3.5})} - 1}{e - 1} \; for \; \widetilde{x} \in [0; 1] \tag{10}$$

where $\widetilde{x}$ is scaled to the length of the relaxation zone.

Irregular wave is represented by a linear superposition of a finite number of individual regular wave components with different amplitudes, frequencies and phases:

$$\eta^{(1)} = \sum_{i=1}^{N} A_i \cos(k_i x - \omega_i t - \varepsilon_i.). \tag{11}$$

where A_i is the amplitude and $Ai = \sqrt{2S(\omega_i)d\omega_i}$, ω_i and ε_i are angular frequency and phase of each component, which is a random number within range $[0, 2\pi]$. Here, a large number of frequency component (2048) is used, and thus the error due to the deterministic calculation of A_i is minimised.

A JONSWAP spectrum is used to describe the distribution of the wave energy as a function of the angular frequency ω. Wave height H_s, peak angular frequency ω_p, and number of components N are given as input values to the JONSWAP spectrum DNV (2011):

$$S(\omega) = \frac{5}{16} H_s^2 \omega_p^4 \omega_i^{-5} exp\left(-\frac{5}{4}\left(\frac{\omega_i}{\omega_p}\right)^{-4}\right) \gamma^{exp\left(\frac{-(\omega-\omega_p)^2}{2\kappa^2\omega_p^2}\right)} A_\gamma. \tag{12}$$

where the peak-shape parameter $\gamma = 3.3$ and the spectral width parameter κ is 0.07 for $\omega_i \leq \omega_p$ and 0.09 for $\omega_i > \omega_p$. The normalising facor $A_\gamma = 1 - 0.287ln(\gamma)$.

The Mitsuyasu directional spreading function $G(\theta)$ Mitsuyasu (1975*a*) is used for the short-crested sea. It introduces a single shape parameter s and multiplies a normalisation factor $G_0(s)$, as shown in Eqn. (13), where $\theta = \theta_i - \overline{\theta}$ and $\overline{\theta}$ is the principal direction representing the major energy propagation direction and θ_i is the direction of each incident wave components measured counter-clockwise from the principal direction.

$$G(\theta) = G_0(s) \cos^{2s}(\frac{\theta}{2}) \tag{13}$$

where

$$G_0(s) = \frac{1}{\pi} 2^{(2s-1)} \frac{\Gamma^2(s+1)}{\Gamma(2s+1)} \tag{14}$$

By multiplying Eqn. (12) and Eqn. (13), the directional spectrum is obtained. An equal energy method (EEM) is used to discretise the frequency spectrum and the spreading function to prevent phase-locking in the directional wave field and ensure ergodicity Duarte et al. (2014); Jefferys (1987). The method discretises the frequency spectrum and directional spreading function based on equal energy bin, resulting in more components close to the peak frequency and the principal direction. As an analogy, a spectrum energy density function is considered as a probability density function (pdf), its integration results in a cumulative distribution function (cdf), which is divided evenly on y-axis. As an example, a JONSWAP spectrum and Mitsuyasu spreading function are discretised using EEM, with each vertical line representing a component, see Fig. 1 and Fig. 2.

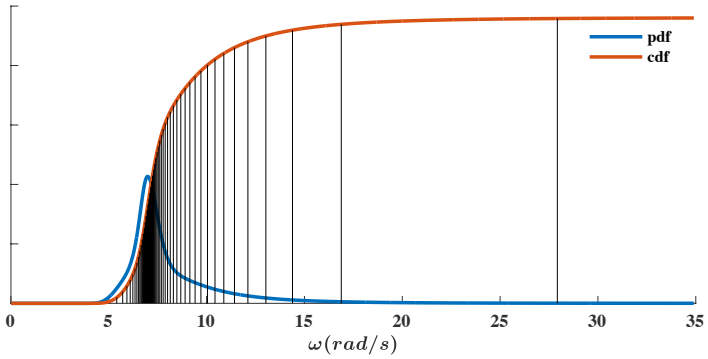

Figure 1: The discretisation of the frequency spectrum based on the Equal Energy method with 50 components.

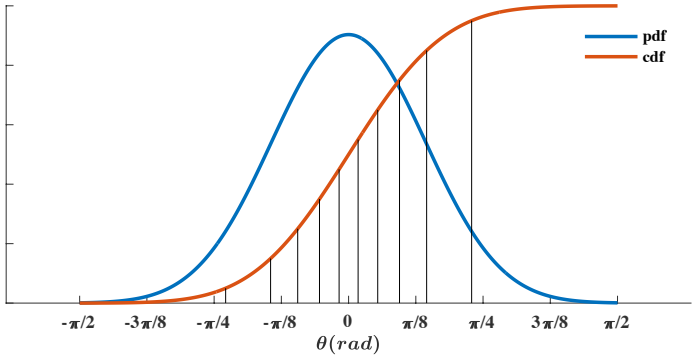

Figure 2: The discretisation of the directional spreading function based on the Equal Energy method with 10 components.

In the offshore area, most wave breaking are steepness-induced. Here, a wave-front steepness criterion is introduced to detect a breaking in the numerical model, as shown in Eqn. 15 Baquet et al. (2017).

$$\frac{\partial \eta}{\partial x_i} \geq \beta. \tag{15}$$

Where $\beta = 1.25$, which is calibrated from the comparison of numerical wave simulation results with model test data Baquet et al. (2017). The horizontal area between the location corresponding to a steepness of 0.1β at the wave-back and the location corresponding to a steepness of β at the wave-front is applied with a viscous damping term to dissipate wave energy in the process Baquet et al. (2017). The breaking algorithm has been used for numerical simulations with different wave steepness and water depth and is seen to be effective in representing irregular wave fields with different wave breaking scenarios Baquet et al. (2017); Huang and Guo (2017); Huang and Zhang (2018); Pakozdi et al. (2020*b*).

4 Results

Numerical wave tank configuration

In the presented study, a full-scale domain is simulated with REEF3D::FNPF. Both the longitudinal and transverse dimensions of the computational domain are 2000 m, the water depth is constant at 600 m. The significant wave height (H_s) and peak period (T_p) of the input wave are 4.5 m and 12.0 s. The JONSWAP spectrum recommended by DNV-GL DNV (2011) and the Mitsuyasu directional spreading function Mitsuyasu (1975*b*) are used to represent the directional spectrum. In the JONSWAP spectrum, the peak-shape parameter $\gamma = 3.3$. A narrow frequency band is used in the study to avoid resolving the wave-wave interaction at lower and higher frequency range, which are not focuses of the presented work. The frequency range of $[0.75\omega_p, 2\omega_p]$ is used, representing about 94.5% of the total wave energy. In the Mitsuyasu directional spreading function, the spreading parameter $s = 10.0$, representing a mildly spreading sea state.

One of the challenges in obtaining the directional spectrum using time-domain information is a correct arrangements of wave gauge arrays. Here, three different types of arrangement are tested: triangle arrangement, pentagon arrangement and heptagon arrangement, as seen in Fig. 3. In each arrangement, a centric wave gauge is located at x=800 m and y=1000 m. The other wave gauges are evenly arranged on a circle around the centric wave gauge with a certain radius. For each arrangement, four different radii in relation to the wavelength corresponding to the peak period (L_p) are used: $0.125L_p$, $0.25L_p$, $0.5L_p$ and L_p. Consequently there are 12 different sets of wave gauge arrays.

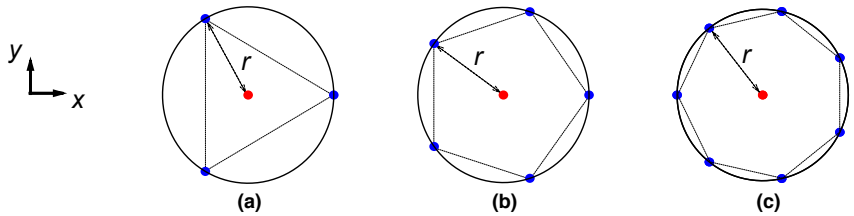

Figure 3: The configurations of wave gauge arrays used to obtain directional spectrum from time series in the 3D numerical wave tank, (a) triangle arrangement, (b)pentagon arrangement, (c)heptagon arrangement.

Another important factor of irregular sea states is that all theories are based on the assumption that ocean is spatially ergodic. Therefore, it is important to show that the simulated area of interest fulfils the assumption. Hypothetically, there is a semi-submersible located at (800, 1000) and it is 120 m long and 120 m wide, roughly the dimension of the biggest semi-submersible Ocean GreatWhite. An area of 25 times of the semi-submersible is numerically investigated to ensure the ergodicity at the site. In this area, 36 wave gauges are arranged in a grid, as shown in Fig. 4. The blue circle is located at (800, 1000), the shaded area represents the semi-submersible, and the red dots are the wave gauge locations.

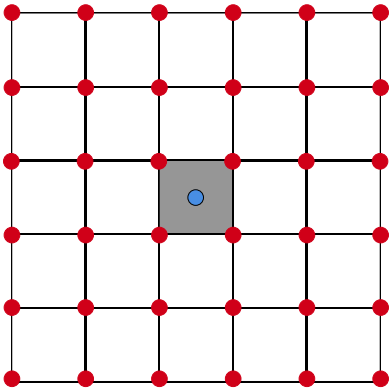

Figure 4: 36 wave gauges (red circles) are arranged in a grid around the hypothetic semi-submersible (shaded area) with a constant distance of 120 m between each other. The coordinate of the blue circle is (800, 1000) m.

With the chosen frequency range, the longest wave and shortest wave components in the wave train have wave lengths of 404.9 m and 60.4 m. As a result, for all the wave components, the chosen scenario is of deep water condition. It is typical to use one wavelength to generate a regular wave using a relaxation zone. Here, a relaxation zone of the longest wave length is used to allow a sufficient distance to generate all wave components Bihs et al. (2016*a*, 2020). Similarly, a numerical beach of the same length is used at the outlet of the numerical wave tank to eliminate reflections. At the side boundaries, symmetric boundary conditions are applied.

Grid convergence study

Previous research Wang et al. (2019) shows that 10 cells in the vertical direction is usually sufficient to represent steep waves using REEF3D::FNPF. Therefore 10 cells are arranged vertically in the current study, a constant-truncation-error method Pakozdi et al. (2019) is used to choose the stretching factor of the stretching function that decides the size of each of the 10 cells so that a correct dispersion relation is ensured in the σ-coordinate system. The peak period and water depth are used as inputs in the method. The optimised grid arrangement for 10 cells is shown in fig. 5. It is seen that the vertical grid arrangement obtained using a stretching factor of 2.875 in REEF3D::FNPF aligns well with the optimal vertical grid arrangement.

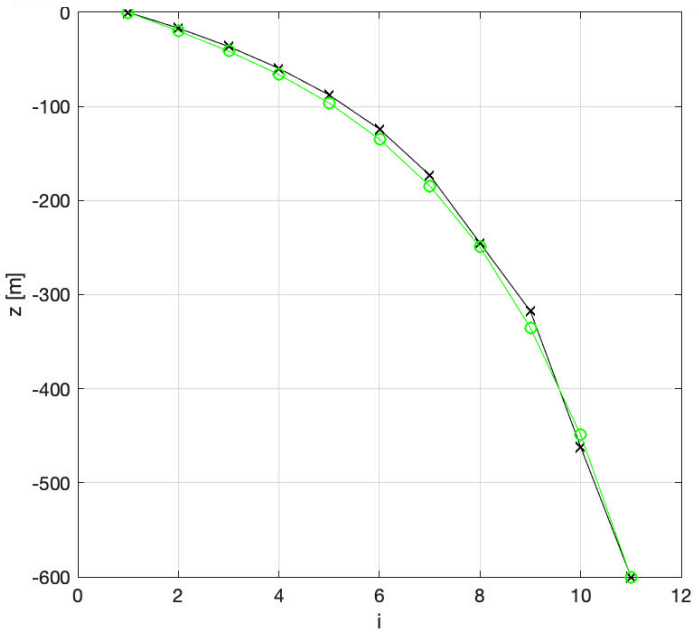

Figure 5: The optimisation of the vertical grid stretching following the constant-truncation-error method Pakozdi et al. (2019). The x-axis is the number of grid and the y-axis shows the water depth. The black line is the theoretical optimal arrangement of the 10 cells in the vertical direction and the green line is the arrangement obtained using the stretching function in REEF3D::FNPF.

In order to resolve all wave components, the horizontal cell size depends on the shortest wave component. For the grid convergence study, uni-directional irregular waves of the same input wave properties are simulated in a two-dimensional numerical wave tank using different grid sizes. There are 7.5 cells per shortest wavelength (L_{min}) in the coarse grid arrangement, 15 cells per L_{min} in the intermediate grid, 30 cells per L_{min} in the fine grid arrangement and 60 cells per L_{min} in a further refinement. For each case, the fixed time step is calculated by dividing the horizontal cell size by the phase velocity of the longest wave component, a method validated by Pakozdi et. al. Pakozdi et al. (2020a). In this way, the flow information is ensured not to jump over a cell within each time step. The resulting time step is 0.08 s. In all cases, 2048 frequency components are used and the waves are simulated for 12800 s, where the three-hour time window between 2000 s and 12800 s are used to produce statistical wave properties. 2000 s allows 300 shortest waves in the wave train to propagate though the NWT and all wave components at anywhere in the NWT reach a quasi-static status, leaving the wave-wave interaction process to a full three-hour time window. The frequency spectra are calculated using the time series recorded at a wave gauge that is located at $x = 800\ m$. The simulated spectra using different grids are compared in Fig. 6. It is seen that the coarse grid underestimates the peak of the spectrum and the intermediate grid overestimates the spectrum peak but looses much energy at higher frequency range. The fine grid produces a frequency spectrum that aligns with the input wave spectrum. The significant wave height H_s from the fine grid is 4.26 m, 98% of the theoretical H_s that corresponds to wave energy within the chosen frequency range. With $L_{min}/dx = 60$, the spectrum is very close to that obtained from

$L_{min}/dx = 30$ without significant further improvements. As a result, $L_{min}/dx = 30$ is used in the following simulations. The spectrum loses certain energy at the high frequency range due to nonlinear wave-wave interactions and breaking waves, which is a common challenge in simulating steep irregular wave fields with a potential flow based numerical model Huang and Guo (2017); Huang and Zhang (2018).

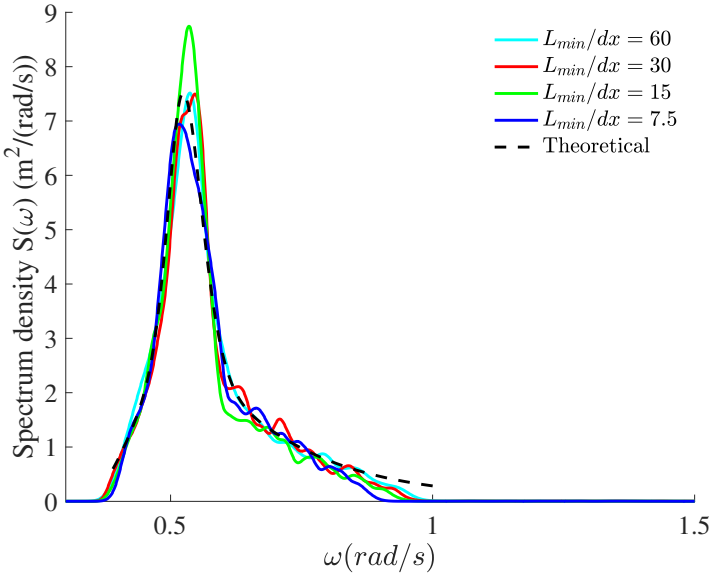

Figure 6: Calculated frequency spectra obtained with different grid sizes in the 2D numerical wave tank.

Simulations of the multi-directional irregular waves

With the chosen resolution from the 2D test, the multi-directional irregular wave propagation is simulated for 12800s in REEF3D::FNPF. 2048 frequency components and 16 directions are used in the simulation. The principal direction is set to be zero degree. The three-hour time series from 2000 s to 128000 s are used for all the statistical analyses. The wave free surface elevation in the numerical wave tank at the last time step is shown in Fig. 7.

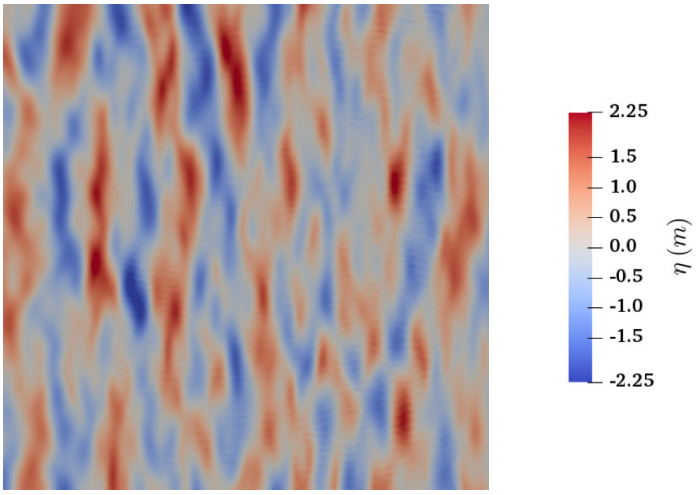

Figure 7: Wave surface elevation in the numerical wave tank with the multi-directional irregular sea state (a zoomed-in area of 1200 m x 1200 m at the centre of the numerical wave tank.)

The significant wave height, peak period, kurtosis and skewness at the 36 wave gauges around the hypothetic semi-submersible are calculated. The relative errors in comparison to the mean values at all wave gauges are plotted in Fig. 8. The relative errors of H_s are all below 5% at any wave gauge, the mean error is 0 and the corresponding variance of error is 3.16e-4. It shows that H_s are almost spatially identical with only minor variations. Similarly, the maximum relative error for T_p is only 5.0%, mean error is 0 and the variance of error is 0.0010. The maximum error for kurtosis is 5.72% and mean error is 0 and the variance is only 9.86e-4. However, a significant variation of skewness is observed in Fig. 8d. The maximum error is found to be 12.24%, the mean of error is 0, and the variance of error is 0.0052, the largest among all investigated quantities. It is also reported by Fouques et. al. (2021) Fouques et al. (2021) that skewness tends to vary more in a nonlinear sea state. Except for the skewness, simulated wave field does not vary much and thus shows a good ergodicity in space.

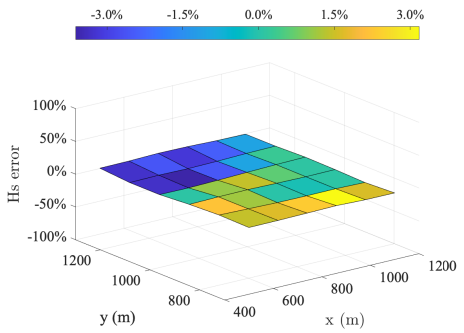

(a) Hs

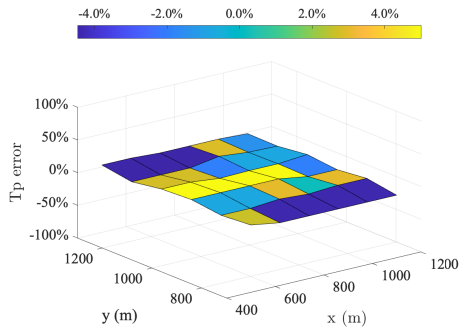

(b) Tp

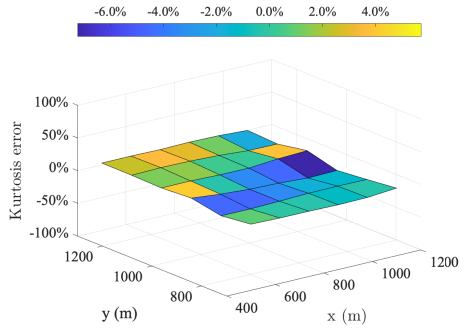

(c) kurtosis

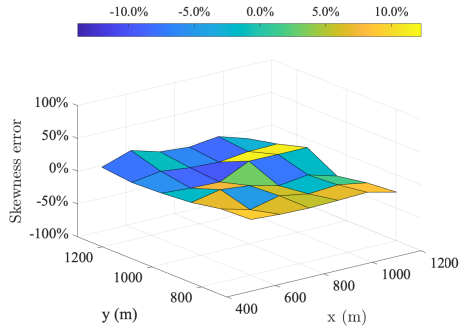

(d) skewness

Figure 8: Spatial variations in terms of relative errors at the 36 wave gauges covering an area 25 times the size of the hypothetic semi-submersible.

A wave number directional spectrum is firstly estimated using FFT for the wave surface elevations at all the grid points in the entire domain at the last time step $t = 12800$ s, as shown in Fig. 9. It is seen that the principal direction is well represented at 0 degree. The directional spreading is symmetric around the principal direction. The wave energy is mainly concentrated within 30 degrees around the principal direction. The wave number at the peak of the spectrum is 0.028, which corresponds to a wavelength of 224.4 m. The wavelength calculated with the peak period is 224.46 m in deep water. Therefore, the peak position is accurately captured in the spectrum too.

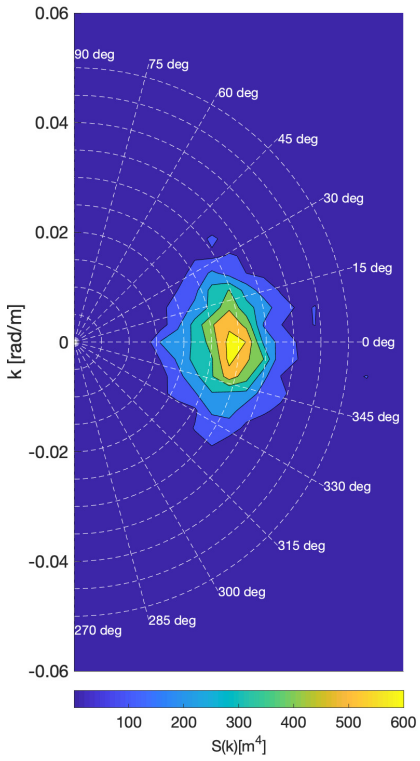

Figure 9: Directional wave number spectrum using FFT in space at $t = 12800s$.

As the ergodicity of the simulated wave field is ensured and the wave number spectrum is well represented, the following analyses focus on the effects of the different wave gauge arrays. Here, the directional spectra are calculated using the time series of the surface elevations at each set of wave gauges in a three-hour duration.

First, the directional spectra reproduced with the triangle arrangement with different radii is presented in Fig. 10. With a radius of $0.125L_p$, the spectrum represents a narrower directional spreading as well as a sharper peak. The spectrum reproduced with a radius of $0.25L_p$ shows that the main wave energy is concentrated within 30 degree around the principal direction. As the radius increases further, the triangle arrangements fails to predict the principal direction, as can be seen from Fig. 10c and Fig. 10d, . It shows that the distance between the wave gauges play an important role when estimating direction spectrum from time series.

A similar correlation between the directional spectrum and the radius of the wave gauge circle is also observed in Fig. 11. Here, a narrower spreading is estimated with $r = 0.125L_p$ and an asymmetric spectrum is produced with $r = L_p$. However, correct directional spreading and peak frequency are represented with both $r = 0.25L_p$ and $r = 0.5L_p$. When the heptagon arrangement is used, a correct principal direction is represented with all radii as seen in Fig. 12. It shows that larger distance between the wave gauges is allowed with an increasing

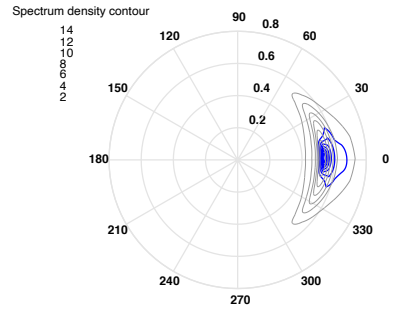

(a)

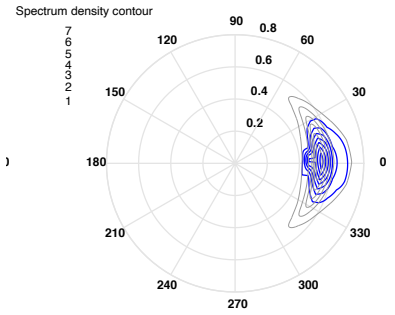

(b)

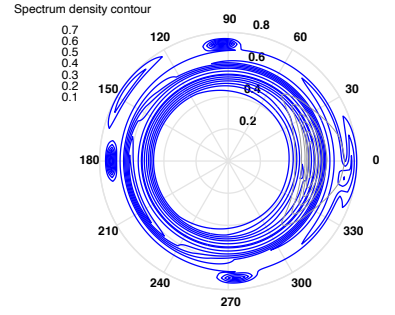

(c)

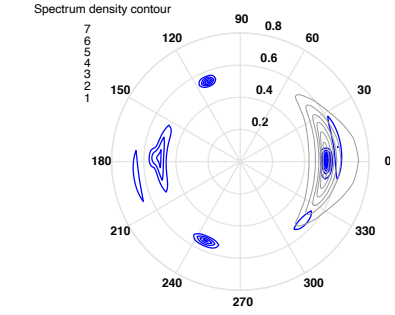

(d)

Figure 10: Directional spectra obtained from the triangle wave gauge arrangement, (a) $r = 0.125L_p$, (b)$r = 0.25L_p$, (c)$r = 0.5L_p$, (d)$r = L_p$. The grey curves represent the theoretical directional spectra.

number of wave gauges.

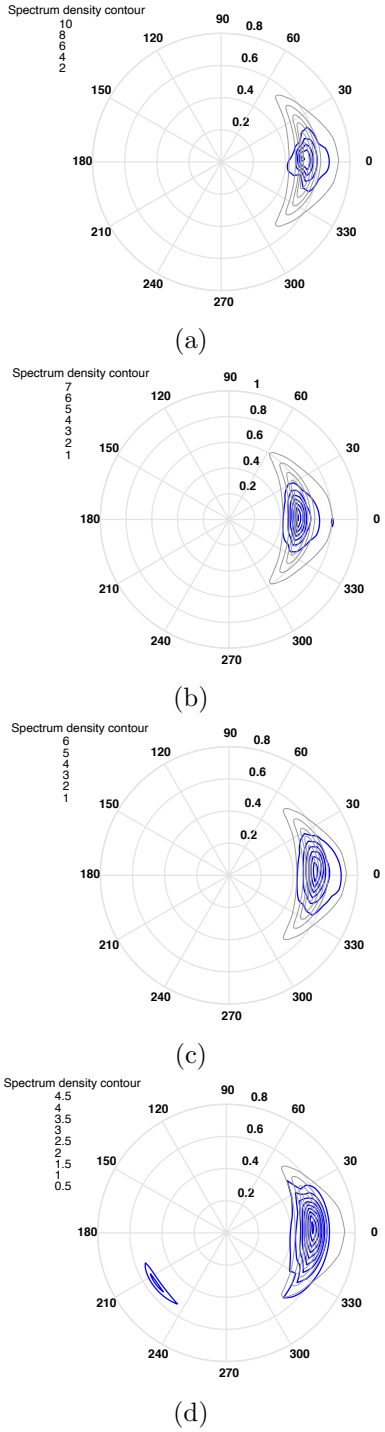

Figure 11: Directional spectra obtained from the pentagon wave gauge arrangement, (a) $r = 0.125L_p$, (b)$r = 0.25L_p$, (c)$r = 0.5L_p$, (d)$r = L_p$. The grey curves represent the theoretical directional spectra.

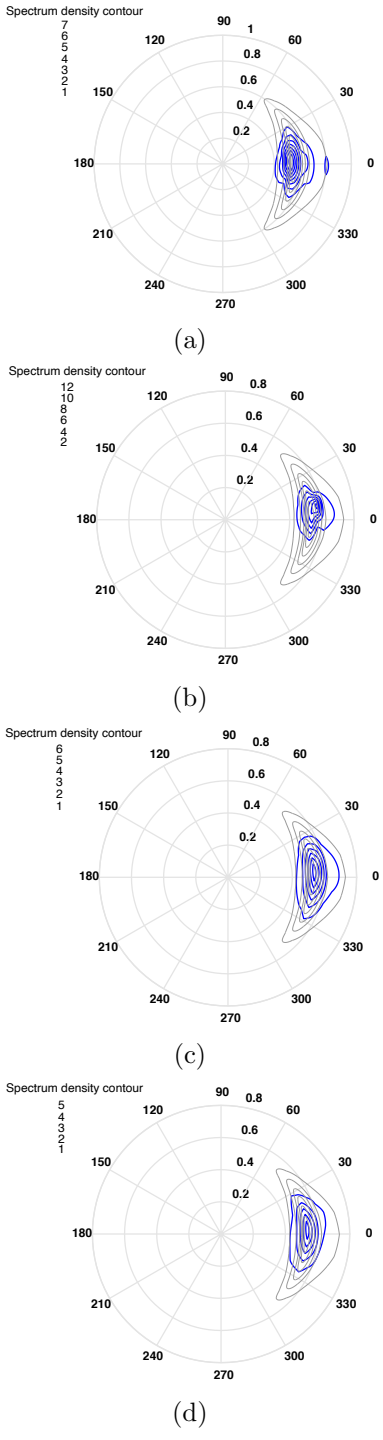

Figure 12: Directional spectra obtained from the heptagon wave gauge arrangement, (a) $r = 0.125L_p$, (b)$r = 0.25L_p$, (c)$r = 0.5L_p$, (d)$r = L_p$. The grey curves represent the theoretical directional spectra.

In the experimental test performed by Nwogu Nwogu (1989) using a 5-gauge arrangement, it is also found that adequate directional information can be found when the radius is smaller than half that of the peak period wavelength. This agrees with the findings in the current study. Therefore, a $0.5L_p$ radius can be considered as maximum radius for the various wave gauge arrays. A $0.25L_p$ radius is seen to be a good practice in general, though the optimal radius might still vary within each arrangement. It is also noticed that reconstructed angular spreading tends to be narrower than the theoretical spectrum though the principal direction and other directional information are correctly represented. The experiments presented by Panicker Panicker and Borgman also indicates that the different arrangements show different angular spreading properties and that the narrower the angular spreading and the higher the peak, the better the resolving spectrum from the wave gauge arrays.

5 Conclusion

In the presented manuscript, the authors explain a procedure of reproducing directional spectrum in a numerical wave tank using the open-source fully nonlinear potential flow model REEF3D::FNPF. The model solves the Laplace equation with boundary conditions on a σ-coordinate system. The arrangement of the vertical grid follows a constant-error method that ensures correct representation of dispersion. The grid resolution in horizontal plane depends on the frequency band. 30 cells or more per shortest wavelength corresponding to the highest frequency is recommended. For extreme sea states where the occurrence of steep and near-breaking waves is high, the horizontal resolution might be subject to further refinement. The fixed time step is calculated by dividing the horizontal cell size by the phase velocity of the longest wave corresponding to the lowest frequency. In all the presented simulations, the three-hour time window for analysis starts after 2000 s to ensure a quasi-static status at all wave gauges. An equal energy method is used in the generation of the multi-directional irregular wave field to avoid phase-locking. The spatial distribution of the significant wave height, peak period, kurtosis and skewness show that the wave field is ergodic. A spatial FFT is used to estimate the wave number directional spectrum. Correct principal direction, peak period and directional spreading are reproduced. When estimating directional spectrum from time series from wave gauge arrays, both the configuration of the gauges and the distance between the wave gauges influence the quality of the reproduced spectrum. In general, with more wave gauges are involved, the arrangement is less sensitive to the distance between the gauges. The radius of the wave gauge array is recommended to be between $0.25L_p$ and $0.5L_p$ based on the tested configurations. When a wider frequency band is used, the wave-wave interaction produce more complicated energy transition, a further study will be needed to decide the recommendation for such cases. The reason behind the different results from the triangle arrangement with half the peak period wavelength is hard to be determined in the current study and requires further investigations. A further investigation on damping zone locations, sizes, methods and correlations with computational domain is also suggested to remove uncertainties on the ergodicity of the wave field.

Acknowledgment

The research work has been funded by the Norwegian Public Roads Administration through the E39 fjord crossing project (No. 304624).

References

Aggarwal, A., Bihs, H., Myrhaug, D. and Chella, M.A. (2019*a*). Characteristics of breaking irregular wave forces on a monopile. *Applied Ocean Research*, **90**, 101846. ISSN 0141-1187. -https://doi.org/10.1016/j.apor.2019.06.003.

Aggarwal, A., Bihs, H., Shirinov, S. and Myrhaug, D. (2019*b*). Estimation of breaking wave properties and their interaction with a jacket structure. *Journal of Fluids and Structures*, **91**, 102722. ISSN 0889-9746. -https://doi.org/10.1016/j.jfluidstructs.2019.102722.

Baquet, A., Kim, J. and Huang, Z.J. (2017). Numerical Modeling Using CFD and Potential Wave Theory for Three-Hour Nonlinear Irregular Wave Simulations. volume Volume 1: Offshore Technology of *International Conference on Offshore Mechanics and Arctic Engineering*. -10.1115/OMAE2017-61090. V001T01A002.

Benoit, M. and Teisson, C. (1994). Laboratory comparison of directional wave measurement systems and analysis techniques. In: *Coastal Engineering 1994*, 42–56. Kobe, Japan. -10.1061/9780784400890.004.

Bihs, H., Kamath, A., Alagan Chella, M., Aggarwal, A. and Arntsen, O. (2016*a*). A new level set numerical wave tank with improved density interpolation for complex wave hydrodynamics. *Computers Fluids*, **140**(Supplement C), 191 – 208. ISSN 0045-7930. -https://doi.org/10.1016/j.compfluid.2016.09.012.

Bihs, H., Kamath, A., Alagan Chella, M., Aggarwal, A. and Øivind A. Arntsen (2016*b*). A new level set numerical wave tank with improved density interpolation for complex wave hydrodynamics. *Computers Fluids*, **140**, 191 – 208. ISSN 0045-7930. -http://dx.doi.org/10.1016/j.compfluid.2016.09.012.

Bihs, H., Wang, W., Pakozdi, C. and Kamath, A. (2020). REEF3D::FNPF—A flexible fully nonlinear potential flow solver. *Journal of Offshore Mechanics and Arctic Engineering*, **142**(4). ISSN 0892-7219. -10.1115/1.4045915.

Bingham, H.B. and Zhang, H. (2007). On the accuracy of finite-difference solutions for nonlinear water waves. *Journal of Engineering Mathematics*, **58**(1), 211–228. ISSN 1573-2703. -10.1007/s10665-006-9108-4.

Booij, N., Ris, R.C. and Holthuijsen, L.H. (1999). A third-generation wave model for coastal regions, 1. model description and validation. *Journal of Geophysical Research*, **104**, 7649–7666.

Brink, F., Izsák, F. and van der Vegt, J.J.W. (2017). Hamiltonian finite element discretization for nonlinear free surface water waves. *Journal of Scientific Computing*, **73**(1), 366–394. ISSN 1573-7691. -10.1007/s10915-017-0416-9.

Chella, M.A., Bihs, H. and Myrhaug, D. (2019). Wave impact pressure and kinematics due to breaking wave impingement on a monopile. *Journal of Fluids and Structures*, **86**, 94 – 123. ISSN 0889-9746. -https://doi.org/10.1016/j.jfluidstructs.2019.01.016.

DNV (2011). Modelling and analysis of marine operations. Standard DNV-RP-H103, Det Norske Veritas, Veritasveien 1, Høvik, Norway.

Duarte, T., Gueydon, S., Jonkman, J. and Sarmento, A. (2014). Computation of Wave Loads Under Multidirectional Sea States for Floating Offshore Wind Turbines. **Volume 9B: Ocean Renewable Energy**. -10.1115/OMAE2014-24148. V09BT09A023.

Ducrozet, G., Bonnefoy, F., Le Touzé, D. and Ferrant, P. (2016). HOS-ocean: Open-source solver for nonlinear waves in open ocean based on High-Order Spectral method. *Computer Physics Communications*, **203**, 245–254. -10.1016/j.cpc.2016.02.017.

Ducrozet, G., Bonnefoy, F., Le Touzé, D. and Ferrant, P. (2012). A modified high-order spectral method for wavemaker modeling in a numerical wave tank. *European Journal of Mechanics - B/Fluids*, **34**, 19–34. ISSN 0997-7546. -https://doi.org/10.1016/j.euromechflu.2012.01.017.

Engsig-Karup, A., Bingham, H. and Lindberg, O. (2009). An efficient flexible-order model for 3D nonlinear water waves. *Journal of Computational Physics*, **228**, 2100–2118.

Fouques, S., Croonenborghs, E., Lim, H., Kim, J., Canard, M., Ducrozet, G., Bouscasse, B., Koop, A., Zhao, B., Wang, W. and Bihs, H. (2021). Qualification criteria for the verification of numerical waves - part 1: potential-based numerical wave tank (PNWT). volume Volume 6: CFD Modeling Practice and Verification of *International Conference on Offshore Mechanics and Arctic Engineering*. Virtual, Online.

Grilli, S.T., Guyenne, P. and Dias, F. (2001). A fully non-linear model for three-dimensional overturning waves over an arbitrary bottom. *International Journal for Numerical Methods in Fluids*, **35**(7), 829–867. -10.1002/1097-0363(20010415)35:7¡829::AID-FLD115¿3.0.CO;2-2.

Grilli, S.T. and Horrillo, J. (1997). Numerical generation and absorption of fully nonlinear periodic waves. *Journal of Engineering Mechanics*, **123**(10), 1060–1069.

Grilli, S.T., Subramanya, R., Svendsen, I.A. and Veeramony, J. (1994). Shoaling of solitary waves on plane beaches. *Journal Waterway Port Coastal and Ocean Enigneering*, **120**(6), 609–628.

Huang, Z. and Zhang, Y. (2018). Semi-empirical single realization and ensemble crest distributions of long-crest nonlinear waves. volume Volume 1: Offshore Technology of *International Conference on Offshore Mechanics and Arctic Engineering*. Madrid, Spain. -10.1115/OMAE2018-78192. V001T01A032.

Huang, Z.J. and Guo, Q. (2017). Semi-empirical crest distributions of long-crest nonlinear waves of three-hour duration. volume Volume 1: Offshore Technology of *International Conference on Offshore Mechanics and Arctic Engineering*. Trondheim, Norway. -10.1115/OMAE2017-61226. V001T01A038.

Jacobsen, N.G., Fuhrman, D.R. and Fredsøe, J. (2012). A wave generation toolbox for the open-source CFD library: OpenFOAM. *International Journal for Numerical Methods in Fluids*, **70**(9), 1073–1088.

Jefferys, E. (1987). Directional seas should be ergodic. *Applied Ocean Research*, **9**(4), 186–191. ISSN 0141-1187. -https://doi.org/10.1016/0141-1187(87)90001-0.

Jiang, G.S. and Shu, C.W. (1996). Efficient implementation of weighted ENO schemes. *Journal of Computational Physics*, **126**, 202–228.

Li, B. and Fleming, C.A. (1997). A three dimensional multigrid model for fully nonlinear water waves. *Coastal Engineering*, **30**(3), 235–258. ISSN 0378-3839. -https://doi.org/10.1016/S0378-3839(96)00046-4.

Ma, Q. and Yan, S. (2006). Quasi ALE finite element method for nonlinear water waves. *Journal of Computational Physics*, **212**(1), 52–72. ISSN 0021-9991. -https://doi.org/10.1016/j.jcp.2005.06.014.

Ma, Q.W., Wu, G.X. and Eatock Taylor, R. (2001*a*). Finite element simulation of fully non-linear interaction between vertical cylinders and steep waves. part 1: methodology and numerical procedure. *International Journal for Numerical Methods in Fluids*, **36**(3), 265–285. -https://doi.org/10.1002/fld.131.

Ma, Q.W., Wu, G.X. and Eatock Taylor, R. (2001*b*). Finite element simulations of fully non-linear interaction between vertical cylinders and steep waves. part 2: numerical results and validation. *International Journal for Numerical Methods in Fluids*, **36**(3), 287–308. -https://doi.org/10.1002/fld.133.

Madsen, P.A., Murray, R. and Sørensen, O.R. (1991). A new form of the Boussinesq equations with improved linear dispersion characteristics. *Coastal Engineering*, **15**, 371–388.

Mayer, S., Garapon, A. and Sørensen, L.S. (1998). A fractional step method for unsteady free surface flow with applications to non-linear wave dynamics. *International Journal for Numerical Methods in Fluids*, **28**, 293–315.

Mitsuyasu, H. (1975*a*). Observations of the directional spectrum of ocean waves using a clover-leaf buoy. *Journal of Physical Oceangraphy*, 750–760.

Mitsuyasu, H. (1975*b*). Observations of the directional spectrum of ocean waves using a clover-leaf buoy. *Journal of Physical Oceangraphy*, 750–760.

Nwogu, O. (1989). Maximum entropy estimation of directional wave spectra from an array of wave probes. *Applied Ocean Research*, **11**(4), 176 – 182. ISSN 0141-1187. -https://doi.org/10.1016/0141-1187(89)90016-3.

Nwogu, O. (1993). Alternative form of Boussinesq equations for nearshore wave propagation. *Journal of Waterways, Port, Coastal, and Ocean Engineering*, **119**(6), 618–638.

Ochi, M.K. (1998). *Ocean Waves: The Stochastic Approach*. Cambridge University Press. ISBN 9780521017671.

Pakozdi, C., Fouques, S., Thys, M., Kamath, A., Wang, W., Dadmarzi, F.H., Bachynski, E. and Bihs, H. (2020*a*). Validation of numerical wave tank simulations using reef3d with jonswap spectra in intermediate water depth. volume Volume 1: Offshore Technology of *International Conference on Offshore Mechanics and Arctic Engineering*. Virtual, Online. -10.1115/OMAE2020-18298. V001T01A012.

Pakozdi, C., Kamath, A., Wang, W. and Bihs, H. (2020*b*). Representation of breaking wave kinematics in the fully nonlinear potential flow model REEF3D::FNPF. volume Volume 8: CFD and FSI of *International Conference on Offshore Mechanics and Arctic Engineering*. Virtual, Online. -10.1115/OMAE2020-18160. V008T08A011.

Pakozdi, C., Wang, W., Kamath, A. and Bihs, H. (2019). Definition of the vertical spacing of a sigma grid based on the constant truncation error. In: *10th National Conference on Computational Mechanics, MekIT19*.

Panicker, N.N. and Borgman, L.E. (????). *Directional Spectra from Wave-Gage Arrays*, chapter 8, 117–136. -10.1061/9780872620285.008.

Shao, Y.L. and Faltinsen, O. (2014*a*). Fully-nonlinear wave-current-body interaction analysis by a harmonic polynomial cell method. *Journal of Offshore Mechanics and Arctic Engineering*, **136**(3), 031301. -10.1115/1.4026960.

Shao, Y.L. and Faltinsen, O.M. (2012). Towards Efficient Fully-Nonlinear Potential-Flow Solvers in Marine Hydrodynamics. volume Volume 4: Offshore Geotechnics; Ronald W. Yeung Honoring Symposium on Offshore and Ship Hydrodynamics of *International Conference on Offshore Mechanics and Arctic Engineering*, 369–380. -10.1115/OMAE2012-83319.

Shao, Y.L. and Faltinsen, O.M. (2014*b*). A harmonic polynomial cell (hpc) method for 3d laplace equation with application in marine hydrodynamics. *Journal of Computational Physics*, **274**, 312–332. ISSN 0021-9991. -https://doi.org/10.1016/j.jcp.2014.06.021.

Shu, C.W. and Osher, S. (1988). Efficient implementation of essentially non-oscillatory shock capturing schemes. *Journal of Computational Physics*, **77**, 439–471.

Stansberg, C.T. (1998). *On the Fourier Series Decomposition of Directional Wave Spectra*, 8. International Society of Offshore and Polar Engineers, Montreal, Canada.

Tannuri, E.A., Mello, P.C., Sales, J.S., Simos, A.N. and Matos, V.L.F. (2007). Estimation of directional wave spectrum using a wave-probe array. *Marine Systems & Ocean Technology*, **3**(2), 123–129. ISSN 2199-4749. -10.1007/BF03449221.

van der Vorst, H. (1992). BiCGStab: A fast and smoothly converging variant of Bi-CG for the solution of nonsymmetric linear systems. *SIAM Journal of Scientific Computing*, **13**, 631–644.

Wang, W., Kamath, A., Pákozdi, C. and Bihs, H. (2019). Investigation of focusing wave properties in a numerical wave tank with a fully nonlinear potential flow model. *Journal of Marine Science and Engineering*, **7**(10), 375. -https://doi.org/10.3390/jmse7100375.

Yates, M.L. and Benoit, M. (2015). Accuracy and efficiency of two numerical methods of solving the potential flow problem for highly nonlinear and dispersive water waves. *International Journal for Numerical Methods in Fluids*, **77**(10), 616–640. -10.1002/fld.3992.